

## Effect of the Coulomb force on fission fragment angular momenta

Jørgen Randrup 

*Nuclear Science Division, Lawrence Berkeley National Laboratory, Berkeley, California 94720, USA*



(Received 5 September 2023; accepted 1 December 2023; published 15 December 2023)

Nuclear fission produces fragments endowed with typically half a dozen units of angular momentum. After scission has occurred, the fragments are still interacting via the Coulomb force which exerts a torque on deformed fragments, thereby accelerating their rotations. The essential features of this effect can be understood by simple perturbative considerations from which the effect on the fragment spin distributions can be obtained. Complete dynamical calculations of the coupled evolution of the spins validate the perturbative treatment, which ignores the second-order terms, showing that the fragment spins evolve essentially independently in the presence of the Coulomb torques.

DOI: [10.1103/PhysRevC.108.064606](https://doi.org/10.1103/PhysRevC.108.064606)

### I. INTRODUCTION

Nuclear fission is a very active topic both theoretically and experimentally [1–7]. Current attention has been particularly focused on the generation (and detection) of the angular momenta of the fission fragments [8–20]. The present study is focused on the effect on the angular momenta of the post-scission Coulomb interaction between the two receding fragments. This topic has been addressed several times in the past [21–24], with mutually conflicting conclusions being reached. The mechanism has generally been ignored in fission treatments, but recent investigations from various perspectives [11,25–27] have suggested that it may in fact be important. The present study seeks to clarify this issue.

For this purpose, the present study considers the dynamical evolution of a pair of rotating fission fragments from right after they have been formed at scission, taking account of their mutual Coulomb repulsion which may increase their angular momenta as they recede.

### II. INTERACTION ENERGY

The first step is to calculate the interaction energy between the two fission fragments,  ${}^{A_L}Z_L$  and  ${}^{A_H}Z_H$ , due to their mutual electrostatic (Coulomb) repulsion. It is assumed that the fragments have uniform charge distributions within their sharp surfaces,  $\rho_f(\mathbf{r}_f)$ . Because the present study is exploratory, only pure quadrupole shapes are considered, notwithstanding that a recent study [27] found that octupole deformations could also play a significant role. Then, in polar coordinates with the fragment symmetry axis as the polar direction, the general expression [28] for the distance from the center of fragment  $f = L, H$  to its surface in the direction  $(\vartheta_f, \varphi_f)$  simplifies

$$d_f(\vartheta_f) = \tilde{R}_f [1 + \tilde{\beta}_f P_2(\cos \vartheta_f)]. \quad (1)$$

The normalization condition,  $\int \rho_f(\mathbf{r}_f) d^3 \mathbf{r}_f = Z_f e$ , yields

$$\tilde{R}_f^3 = R_f^3 / [1 + \frac{3}{5} \tilde{\beta}_f^2 + \frac{2}{35} \tilde{\beta}_f^3], \quad (2)$$

where the standard “equivalent sharp” nuclear radius is  $R_f = (1.15 \text{ fm}) A_f^{1/3}$  [29]. The convenient deformation parameter  $\tilde{\beta}$  is related to the more familiar parameter  $\beta_{20}$  (see, e.g., Refs. [29,30]) by  $\tilde{\beta} = \sqrt{5/4\pi} \beta_{20}$ .

The associated Coulomb interaction energy is

$$V = \int \frac{\rho_L(\mathbf{r}_L) \rho_H(\mathbf{r}_H)}{|\mathbf{R} + \mathbf{r}_L - \mathbf{r}_H|} d^3 \mathbf{r}_L d^3 \mathbf{r}_H, \quad (3)$$

where  $\mathbf{R} = \mathbf{R}_L - \mathbf{R}_H = (R, \Theta, \Phi)$  is the separation between the two fragment centers. With the fragment orientations being  $(\Theta_f, \Phi_f)$ , the interaction energy, through second order in the deformations  $\tilde{\beta}_f$ , was derived by Denisov and Pilipenko [31],

$$V(R, \theta_L, \theta_H, \phi) = e^2 \frac{Z_L Z_H}{R} [1 + \tilde{\beta}_L \tilde{f}_1^{(L)} + \tilde{\beta}_H \tilde{f}_1^{(H)} + \tilde{\beta}_L^2 \tilde{f}_2^{(L)} + \tilde{\beta}_H^2 \tilde{f}_2^{(H)} + \tilde{\beta}_L \tilde{\beta}_H (\tilde{f}_3 + \tilde{f}_4)]. \quad (4)$$

where  $\theta_f \equiv \Theta_f - \Theta$  and  $\phi \equiv \Phi_L - \Phi_H$ . The  $\tilde{f}$  coefficients are given by

$$\begin{aligned} \tilde{f}_1^{(f)} &= \frac{3}{5} \xi_f^2 P_2(c_f), \quad \tilde{f}_2^{(f)} = \frac{12}{35} \xi_f^2 P_2(c_f) + \frac{18}{35} \xi_f^4 P_4(c_f), \\ \tilde{f}_3 &= \frac{27}{100} \xi_L^2 \xi_H^2 [17 c_L^2 c_H^2 - 5 c_L^2 - 5 c_H^2 + 1], \\ \tilde{f}_4 &= \frac{27}{50} \xi_L^2 \xi_H^2 [s_L^2 s_H^2 \cos^2 \phi - 2 \sin 2\theta_L \sin 2\theta_H \cos \phi], \end{aligned} \quad (5)$$

where  $c_f \equiv \cos \theta_f$ ,  $s_f \equiv \sin \theta_f$ , and  $\xi_f \equiv \tilde{R}_f/R$ .

The main effect of the interaction potential  $V$  is the acceleration of the fragment separation,  $\mu \dot{\mathbf{R}} = -\partial V / \partial \mathbf{R}$ , as manifested in the total kinetic energy of the fragments. In addition, the orientation of a deformed fragment,  $\hat{\omega}_f = (\Theta_f, \Phi_f)$ , is subject to a torque that causes its angular momentum  $\mathbf{S}_f$  to change,  $\dot{\mathbf{S}}_f = -\partial V / \partial \hat{\omega}_f$ . This latter effect is the focus of the present study.

### III. PHYSICAL SCENARIO

As is evident from the above expression (4) for  $V$ , the torques are proportional to the product of the fragment charges,  $Z_L Z_H$  and, to leading order, to the deformation  $\tilde{\beta}_f$  of the fragment considered. Therefore, in order to obtain an upper bound on effect, the study considers fission of californium, which is the most highly charged system for which it is practical to carry out experiments. Furthermore, it focuses on one particular fission channel,  $^{252}\text{Cf} \rightarrow ^{98}\text{Sr} + ^{154}\text{Nd}$ , where both fragments are well deformed. Ignoring possible early distortions of the fledging fragments, we employ the calculated ground-state quadrupole deformations given in Ref. [30],  $\beta_{20}(^{98}\text{Sr}) = 0.352$  and  $\beta_{20}(^{154}\text{Nd}) = 0.270$ , and thus use  $\tilde{\beta}(^{98}\text{Sr}) = 0.222$  and  $\tilde{\beta}(^{154}\text{Nd}) = 0.170$ . Approximate results for other cases can be obtained by suitable scaling of the results presented here (see later).

The present study assumes that the fragments are initially (i.e., right after scission has been completed) coaxial,  $\theta_L = \theta_H = 0$ , and their center separation  $R_0$  is adjusted such that their Coulomb interaction energy is  $\text{TKE}(^{98}\text{Sr} + ^{154}\text{Nd}) = 174.35$  MeV. (This value was obtained with the fission event generator FREYA [32] based on the measured mean total fragment kinetic energy for the considered mass partition [33]; the precise value is not important in the present context.) For this configuration, the point-charge energy is  $V_0 = e^2 Z_L Z_H / R_0 = 170.51$  MeV, while the first- and second-order contributions in Eq. (4) are 3.46 and 0.54 MeV, respectively. These numbers suggest that the effect is relatively small and, furthermore, that the first-order contribution alone will provide a good approximation (which will prove to be correct).

An impression of the orientation dependence of the interaction energy can be gained from Fig. 1 which shows contours of  $V(R, \theta_L, \theta_H, \phi)$  for  $R = R_0$  and  $\phi = 0$ . The full potential given in Eq. (4) as well as the contributions through first order are shown. As can be seen, the first-order truncation provides a good approximation to the full potential.

Generally  $V$  has a minimum at  $\theta_L = \theta_H = 90^\circ$ , where the fragments are oriented perpendicular to the fission axis and the Coulomb torques vanish, and it attains its maximum value for the coaxial configuration where  $\theta_f$  are either  $0^\circ$  or (equivalently)  $180^\circ$  and the torques also vanish. Furthermore,  $V$  increases steadily as  $\theta_L$  moves away from  $90^\circ$  for a given  $\theta_H$ , and vice versa. At  $R = R_0$ , the variation in  $V$  as  $\theta_f$  is changed from  $0^\circ$  to  $180^\circ$  is typically about 3 MeV, corresponding to  $\approx 1.7\%$ , whereas the amplitude of the variation in  $V$  as a function of  $\phi$  is smaller than that by a factor of  $\approx 30$  and its relative magnitude quickly diminishes as the fragments separate. In fact, the contours corresponding to  $\phi = 0^\circ$  (shown on Fig. 1) and those for  $\phi = 90^\circ$  are hardly distinguishable to the eye. Thus the dependence of  $V$  on the azimuthal orientations of the fragments is not expected to be important.

### IV. PERTURBATIVE ANALYSIS

As suggested by Fig. 1, the Coulomb interaction potential between the deformed fragments is to a good approximation given by just the first-order terms in Eq. (4), i.e., those proportional to  $\tilde{\beta}_L$  and  $\tilde{\beta}_H$ . Consequently, the effect of the post-scission Coulomb interaction on the angular momentum

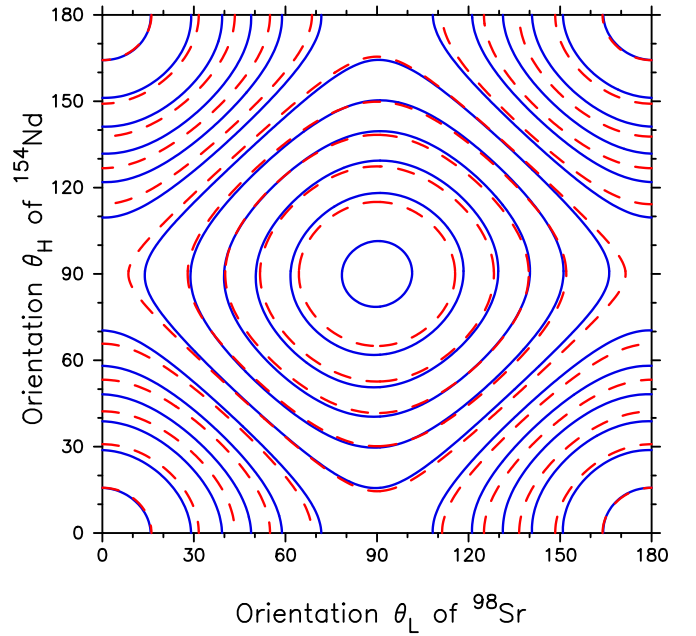


FIG. 1. Contour plot of the Coulomb interaction potential between the fragments  $^{98}\text{Sr}$  and  $^{154}\text{Nd}$  placed at their initial center separation  $R_0$ , as a function of their in-plane orientations  $\theta_L$  and  $\theta_H$ ,  $V(R_0, \theta_L, \theta_H, 0)$ , calculated with either all terms included (solid blue) or only to first order in  $\tilde{\beta}_L$  and  $\tilde{\beta}_H$  (dashed red); the contours are separated by 0.5 MeV.

of one fragment is practically independent of the deformation and orientation of the other fragment.

It is therefore possible to obtain a good understanding of the effect on the basis of a simple perturbative analysis. For this we consider the torque exerted on a steadily rotating deformed fragment as it recedes radially from its partner, ignoring the deformation of the partner as well as the relatively slow counter rotation of the dinuclear axis  $\hat{\mathbf{R}}$  dictated by angular momentum conservation. The relative motion is then purely radial,  $\mathbf{R}(t) = (R(t), 0, 0)$ , with  $\mu\dot{\mathbf{R}} = \dot{\mathbf{P}} = -\partial V / \partial \mathbf{R}$  and the torque is given by

$$\tau_f \equiv -\frac{\partial V}{\partial \Theta_f} \approx -e^2 \frac{Z_L Z_H}{R} \tilde{\beta}_f \frac{\partial \tilde{f}_1^{(f)}}{\partial \theta_f}, \quad (6)$$

where

$$\frac{\partial \tilde{f}_1^{(f)}}{\partial \theta_f} = -\frac{9}{10} \frac{\tilde{R}_f^2}{R(t)^2} \sin 2\theta_f(t). \quad (7)$$

Because the perturbative treatment assumes that the angular frequency  $\omega_f = S_f / \mathcal{I}_f$  remains constant, the orientation angle increases steadily,  $\theta_f(t) = \omega_f t$ .

Figure 2 displays these torques for each of the two fragments for a range of angular momenta  $S$ . Generally, the torque exhibits a damped oscillation as a function of time. At early times, shortly after scission has been completed, the fragment rotation has not proceeded very far,  $\theta_f \ll 45^\circ$ , nor has the separation  $R$  yet grown significantly above  $R_0$ , so the torque increases roughly in proportion to  $\sin 2\theta_f$ . However, the accelerating growth of  $R$  causes the torque to peak well before the optimal orientation of  $\theta_f = 45^\circ$  has been reached. Once

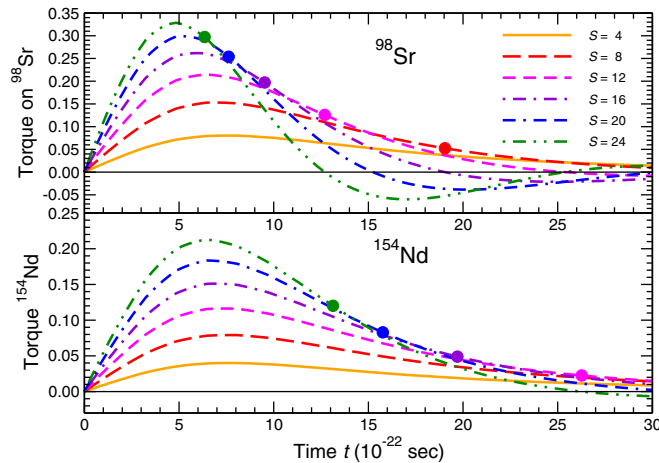


FIG. 2. The time-dependent torque exerted on a deformed fragment ( $^{98}\text{Sr}$  or  $^{154}\text{Nd}$ ) as it recedes from its partner ( $^{154}\text{Nd}$  or  $^{98}\text{Sr}$ ). It is assumed that the fragment moves radially and keeps rotating with a constant angular frequency,  $\omega = S/\mathcal{I}$  with  $S = 4, 8, 12, 16, 20, 24 \hbar$ , while the partner is kept stationary and spherical. The solid symbols are placed on the curves when the fragment orientation has reached  $\theta = 45^\circ$ .

$\theta_f$  has passed  $45^\circ$ , the increasingly unfavorable orientation together with the ever larger  $R$  causes the torque to decrease more rapidly. It changes sign when  $\theta_f$  passes  $90^\circ$ .

The gain in angular momentum,  $\Delta S = S' - S$ , can be obtained approximately as the time integral of the torque discussed above [see Eq. (6)],

$$\Delta S_f = \int \tau_f dt = \frac{9}{10} e^2 Z_L Z_H \tilde{\beta}_f \tilde{R}_f^2 \int_0^\infty \frac{\sin 2\theta_f t}{R(t)^3} dt. \quad (8)$$

The resulting  $\Delta S$  is shown in Fig. 3 as a function of  $S$ . For small angular momenta, where the fragment separation dominates over the fragment rotation and the maximum torque occurs well before the fragment has turned very far, the angular momentum gain  $\Delta S$  increases with  $S$ . In the opposite extreme of very large angular momenta, the rotation dominates over the separation and the fragment can

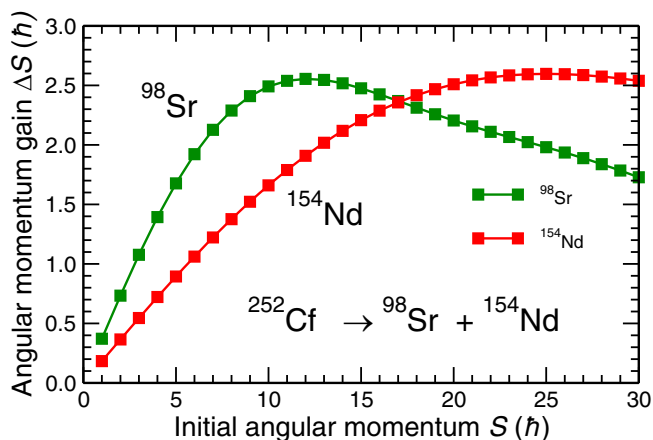


FIG. 3. The gain in angular momentum,  $\Delta S = S' - S$ , as obtained with the perturbative calculation using the time-dependent torques displayed in Fig. 2.

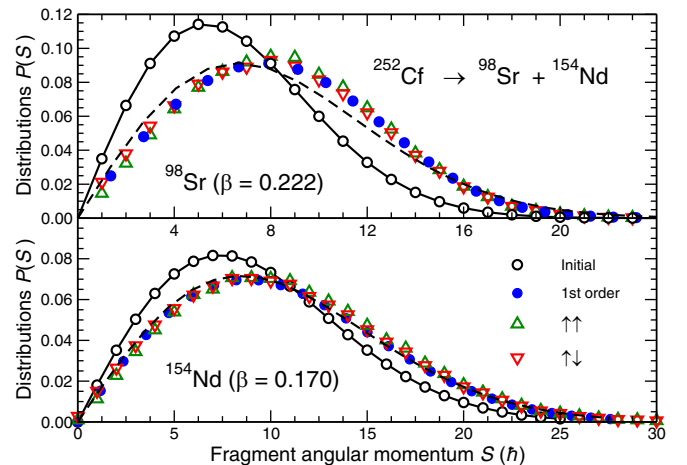


FIG. 4. The distribution of pre- and post-Coulomb angular momenta for the fragments  $^{98}\text{Sr}$  (top) and  $^{154}\text{Nd}$  (bottom) from the reaction  $^{252}\text{Cf} \rightarrow ^{98}\text{Sr} + ^{154}\text{Nd}$ , as obtained by either the perturbative calculation (blue solid circles) or by solving the complete coupled equations for  $10^4$  sampled events as described in the text, with the two fragment spins being either parallel (green triangles pointing up) or antiparallel (red triangles pointing down). For each of the fragments, the dashed curve is the statistical distribution that has the same rms width. The initial statistical distributions of the angular momentum magnitudes are indicated by solid curves with the open circles.

complete several full rotations before the separation has increased significantly. The associated cancellation then causes  $\Delta S$  to decrease with  $S$ . For Sr a maximum gain of  $\approx 2.6 \hbar$  occurs at  $S \approx 12 \hbar$ , while Nd receives a similar maximum gain at  $S \approx 25 \hbar$ .

It should be noted that the dependence of  $\Delta S$  on  $S$  and  $\mathcal{I}$  is only through their ratio  $\omega = S/\mathcal{I}$ . Therefore a reduction of the moment of inertia,  $\mathcal{I} \rightarrow \mathcal{I}/c$ , will yield the same  $\Delta S$  as a corresponding increase of the initial spin,  $S \rightarrow cS$ . Thus, with a rescaling of the abscissa, Fig. 3 would apply to such a modified scenario as well.

Furthermore, to a good approximation, the effect of the Coulomb torque on the fragment spin is proportional to the deformation of the fragment. [The torque itself is proportional to  $\tilde{\beta}_f$  (to first order), but because the moment of inertia  $\mathcal{I}_f$  increases with  $\tilde{\beta}_f$ , the rotational frequency is affected which in turn changes the effective time over which the torque acts, thereby causing a slight deviation from a strict proportionality.] Therefore the results shown here can readily be used to estimate the effects for cases other than the one exhibited here ( $^{252}\text{Cf} \rightarrow ^{98}\text{Sr} + ^{154}\text{Nd}$ ).

In the present scenario, where the initial fragment spins are sampled microcanonically, the distributions of their magnitudes have a canonical form,  $P_f(S) \sim S \exp(-S^2/2\sigma_f^2)$ , which yields  $\sigma_{\text{Sr}} = 5.30 \hbar$  and  $\sigma_{\text{Nd}} = 7.42 \hbar$ . After the Coulomb torques have changed the spins, their distributions  $P'_f(S')$  are no longer canonical, because the degree of magnification,  $S'/S$ , is not a constant (see Fig. 3), and the relative weight of the larger angular momenta has been enhanced. This is illustrated in Fig. 4 by the dashed curves which show canonical distributions with  $\sigma$  values that lead to the same rms spin

as the resulting distribution,  $\sigma'_{\text{Sr}} = 6.64\hbar$  and  $\sigma'_{\text{Nd}} = 8.47\hbar$ . As expected, the deviation from a canonical form is largest for  $^{98}\text{Sr}$ . These results are qualitatively similar to those obtained very recently by Scamps and Bertsch [27] with a quantal treatment of the coupled fragment motion.

## V. COMPLETE TREATMENT

In a realistic description of fission, the initial angular momenta of the two fragments,  $S_L$  and  $S_H$ , fluctuate from event to event. For the present study it is assumed that these angular momenta are perpendicular to the fission axis  $\hat{\mathbf{R}}$ . In order to investigate the effect of the Coulomb interaction on the angular-momentum distribution, the evolution of a large number of individual events is calculated with the initial angular momenta being sampled microcanonically from the correlated joint distribution  $P(S_L, S_H)$ . The specific sampling procedure is not important for the present purpose but, for completeness, it is described in the Appendix.

Generally, the two fragment angular momenta, while both being perpendicular to the fission axis  $\hat{\mathbf{R}}$ , differ in direction by the relative azimuthal angle  $\phi$ . As discussed above, the dependence on  $\phi$  is expected to be unimportant. It is therefore assumed that  $S_L$  and  $S_H$  are either parallel ( $\phi = 0^\circ$ ) or antiparallel ( $\phi = 180^\circ$ ), corresponding to the largest possible azimuthal difference. Then the two fragment axes remain in the same plane as that of the relative motion, i.e., the fragment angular momenta  $S_L$  and  $S_H$  as well as the relative angular momentum  $L$  are all parallel (or antiparallel), so only the components along that common direction need to be considered.

Once the initial two-fragment state has been specified, the subsequent evolution of the system is governed by the coupled equations of motion following from Eq. (4),

$$\dot{\mathbf{R}} = \mathbf{P}/\mu \quad \dot{\mathbf{P}} = -\partial V/\partial \mathbf{R}, \quad (9)$$

$$\dot{\Theta}_L = S_L/\mathcal{I}_L \quad \dot{S}_L = -\partial V/\partial \Theta_L, \quad (10)$$

$$\dot{\Theta}_H = S_H/\mathcal{I}_H \quad \dot{S}_H = -\partial V/\partial \Theta_H. \quad (11)$$

These equations can be reliably solved by use of the leap-frog method [34]. For each of the two fragments, the distribution of its initial angular momentum magnitude,  $P_f(S)$ , and that of its final value,  $P'_f(S')$ , can then be obtained by binning the values obtained for the event sample. The resulting distributions are shown in Fig. 4. Several features are noteworthy:

1) For each fragment, the distribution for parallel angular momenta ( $\phi = 0$ ) is very similar to that for anti-parallel angular momenta ( $\phi = \pi$ ), confirming that the azimuthal dependence is rather unimportant and that the two fragment orientations evolve essentially independently.

2) Furthermore, these distributions are rather well approximated by the result of the perturbative treatment, confirming that the higher-order terms in  $V$ , including the quadrupole-quadrupole interaction, play only a minor role.

3) The post-scission Coulomb interaction broadens the angular-momentum distributions significantly. The effect is larger for  $^{98}\text{Sr}$  not only because it is more deformed but also because it tends to rotate faster than  $^{154}\text{Nd}$  (by a factor of  $\approx 2$ ) so it reaches a favorable orientation earlier, while the Coulomb field is still effective (see Fig. 2).

## VI. CONCLUDING REMARKS

The present study indicates that the Coulomb repulsion between two fission fragments may cause a significant increase of their angular momenta. In the idealized scenario studied here, the gains in the peak region of the distribution are  $\Delta S_{\text{Sr}} \approx 1\text{--}2.5\hbar$  and  $\Delta S_{\text{Nd}} \approx 0.6\text{--}2.3\hbar$ , and the overall average increase of the angular momentum magnitude is  $1.8\hbar$  for  $^{98}\text{Sr}$  and  $1.4\hbar$  for  $^{154}\text{Nd}$ .

In the case considered, the fissioning system,  $^{252}\text{Cf}$ , has a particularly large charge,  $Z_0 = 98$ , and the two fragments considered are both well deformed, features that enhance the effect. But, because the angular momentum gained by a fragment is effectively independent of the deformation (and rotation) of the partner fragment, qualitatively similar amplifications should be expected for any deformed fission fragment.

A particularly simple feature is that the amplification of the spin magnitude of a fragment depends on its initial spin and its moment of inertia only through the ratio  $S/\mathcal{I}$ . This extends the applicability of the present results to scenarios where the moments of inertia differ from the rigid values employed here.

Based on the present study, one may conclude that the effect of the Coulomb torque on the angular momenta of the receding fission fragments is significant, though not overwhelming, suggesting that dynamical treatments of fission should include the effect of the Coulomb force in the description of the post-scission dynamics.

However, this presents a delicate challenge because the fragments are distorted away from their equilibrium shapes when they are released and the resulting Coulomb effect is therefore sensitive to the time scale of the subsequent relaxation of the fragment shapes. In principle, this interplay makes it possible to gain information on the shape relaxation dynamics from the final angular momentum distribution.

## ACKNOWLEDGMENTS

The author thanks G. F. Bertsch, V. Yu. Denisov, and R. L. Vogt for stimulating discussions on this topic. This work was supported in part by the Office of Nuclear Physics in the U.S. Department of Energy's Office of Science under Contract No. DE-AC02-05CH11231.

## APPENDIX: ANGULAR MOMENTUM SAMPLING

The two axially symmetric deformed fragments are initially in a coaxial configuration with their center separation being  $R_0$ . The moment of inertia for the relative fragment motion is then  $\mathcal{I}_R = \mu R_0^2$ .

The angular momenta of the fragments are sampled from a correlated statistical distribution,  $P(S_L, S_H)$ , as in the fission event generator FREYA [32]. This is accomplished by first sampling the amplitudes of the two transverse normal modes, wriggling and bending,  $\mathbf{s}_{\text{wrig}} = (s_x^{\text{wrig}}, s_y^{\text{wrig}}, 0)$  and  $\mathbf{s}_{\text{bend}} = (s_x^{\text{bend}}, s_y^{\text{bend}}, 0)$ , from the corresponding thermal distributions

$$P_{\text{wrig}}(\mathbf{s}_{\text{wrig}}) \sim e^{-s_{\text{wrig}}^2/2\mathcal{I}_{\text{wrig}}T}, \quad (\text{A1})$$

$$P_{\text{bend}}(\mathbf{s}_{\text{bend}}) \sim e^{-s_{\text{bend}}^2/2\mathcal{I}_{\text{bend}}T}, \quad (\text{A2})$$

where the moments of inertia for the normal modes are

$$\mathcal{I}_{\text{wrig}} = \frac{\mathcal{I}_0}{\mathcal{I}_R} \mathcal{I}_{LH}, \quad \mathcal{I}_{\text{bend}} = \frac{\mathcal{I}_L \mathcal{I}_H}{\mathcal{I}_{LH}} \quad (\text{A3})$$

with  $\mathcal{I}_{LH} \equiv \mathcal{I}_L + \mathcal{I}_H$  and  $\mathcal{I}_0 \equiv \mathcal{I}_{LH} + \mathcal{I}_R$ . The moments of inertia of the individual fragments,  $\mathcal{I}_L$  and  $\mathcal{I}_H$ , are taken as the rigid-body values,  $\mathcal{I}_f = \frac{2}{5} M_f R_f^2$ . The individual fragment angular momenta can then be constructed subsequently,

$$\mathbf{S}_L = \frac{\mathcal{I}_L}{\mathcal{I}_{LH}} \mathbf{s}_{\text{wrig}} + \mathbf{s}_{\text{bend}}, \quad (\text{A4})$$

$$\mathbf{S}_H = \frac{\mathcal{I}_H}{\mathcal{I}_{LH}} \mathbf{s}_{\text{wrig}} - \mathbf{s}_{\text{bend}}. \quad (\text{A5})$$

The angular momentum of the relative fragment motion,  $\mathbf{L} = \mu \mathbf{R} \times \dot{\mathbf{R}}$ , follows from angular momentum conservation,  $\mathbf{L} = -\mathbf{S}_L - \mathbf{S}_H = -\mathbf{s}_{\text{wrig}}$ . It is assumed that the initial radial motion vanishes,  $\dot{R} = 0$ , so  $\dot{\mathbf{R}}$  follows from  $\mathbf{L}$ .

The individual spin magnitudes have canonical distributions,  $P_f(S) \sim S \exp(-S^2/2\sigma_f^2)$ , but, due to the angular-momentum conservation, the widths are slightly reduced,  $\sigma_f^2 = T \mathcal{I}_f (1 - \mathcal{I}_f/\mathcal{I}_0)$ , and the spin vectors are slightly anti-correlated,  $\langle \mathbf{S}_L \cdot \mathbf{S}_H \rangle = -2T \mathcal{I}_L \mathcal{I}_H / \mathcal{I}_0$ .

For the case considered here,  $^{252}\text{Cf}(\text{sf})$ , FREYA yields an average temperature at scission equal to  $T = 1.0 \text{ MeV}$  for the particular division considered,  $^{98}\text{Sr} + ^{154}\text{Nd}$ . The present illustrative calculations have therefore been carried out using that value.

- 
- [1] N. Schunck and L. M. Robledo, Microscopic theory of nuclear fission: A review, *Rep. Prog. Phys.* **79**, 116301 (2016).
- [2] A. N. Andreyev, K. Nishio, and K.-H. Schmidt, Nuclear fission: A review of experimental advances and phenomenology, *Rep. Prog. Phys.* **81**, 016301 (2018).
- [3] K.-H. Schmidt and B. Jurado, Review on the progress in nuclear fission - experimental methods and theoretical descriptions, *Rep. Prog. Phys.* **81**, 106301 (2018).
- [4] P. Talou *et al.*, Correlated prompt fission data in transport simulations, *Eur. Phys. J. A* **54**, 9 (2018).
- [5] M. Bender *et al.*, Future of nuclear fission theory, *J. Phys. G: Nucl. Part. Phys.* **47**, 113002 (2020).
- [6] N. Schunck and D. Regnier, Theory of nuclear fission, *Prog. Part. Nucl. Phys.* **125**, 103963 (2022).
- [7] *Nuclear Fission: Theories, Experiments and Applications*, edited by P. Talou and R. Vogt (Springer International Publishing, Berlin, 2023).
- [8] G. F. Bertsch, T. Kawano, and L. M. Robledo, Angular momentum of fission fragments, *Phys. Rev. C* **99**, 034603 (2019).
- [9] A. Al-Adili, Z. Gao, M. Lantz, A. Solders, M. Österlund, and S. Pomp, Isomer yields in nuclear fission, *EPJ Web Conf.* **256**, 00002 (2021).
- [10] M. Travar *et al.*, Experimental information on mass-and TKE-dependence of the prompt fission  $\gamma$ -ray multiplicity, *Phys. Lett. B* **817**, 136293 (2021).
- [11] J. N. Wilson *et al.*, Angular momentum generation in nuclear fission, *Nature (London)* **590**, 566 (2021).
- [12] R. Vogt and J. Randrup, Angular momentum effects fission, *Phys. Rev. C* **103**, 014610 (2021).
- [13] A. Bulgac, I. Abdurrahman, S. Jin, K. Godbey, N. Schunck, and I. Stetcu, Fission fragments intrinsic spins and their correlations, *Phys. Rev. Lett.* **126**, 142502 (2021).
- [14] P. Marević, N. Schunck, J. Randrup, and R. Vogt, Angular momentum of fission fragments from microscopic theory, *Phys. Rev. C* **104**, L021601 (2021).
- [15] J. Randrup and R. Vogt, Generation of fragment angular momentum in fission, *Phys. Rev. Lett.* **127**, 062502 (2021).
- [16] S. Marin, M. S. Okar, E. P. Sansevero, I. E. Hernandez, C. A. Ballard, R. Vogt, J. Randrup, P. Talou, A. E. Lovell, I. Stetcu, O. Serot, O. Litaize, A. Chebboubi, S. D. Clarke, V. A. Protopopescu, and S. A. Pozzi, Structure in the event-by-event neutron- $\gamma$  multiplicity correlations in  $^{252}\text{Cf}(\text{sf})$ , *Phys. Rev. C* **104**, 024602 (2021).
- [17] I. Stetcu, A. E. Lovell, P. Talou, T. Kawano, S. Marin, S. A. Pozzi, and A. Bulgac, Angular momentum removal by neutron and  $\gamma$ -ray emissions during fission fragment decays, *Phys. Rev. Lett.* **127**, 222502 (2021).
- [18] S. Marin, E. P. Sansevero, M. S. Okar, I. E. Hernandez, R. Vogt, J. Randrup, S. D. Clarke, V. A. Protopopescu, and S. A. Pozzi, Directional dependence of the event-by-event neutron- $\gamma$  multiplicity correlations in  $^{252}\text{Cf}(\text{sf})$ , *Phys. Rev. C* **105**, 054609 (2022).
- [19] J. Randrup, T. Døssing, and R. Vogt, Probing fission fragment angular momenta by photon measurements, *Phys. Rev. C* **106**, 014609 (2022).
- [20] A. Bulgac, I. Abdurrahman, K. Godbey, and I. Stetcu, Fragment intrinsic spins and fragments relative orbital angular momentum in nuclear fission, *Phys. Rev. Lett.* **128**, 022501 (2022).
- [21] J. O. Rasmussen, W. Nörenberg, and H. J. Mang, A model for calculating the angular momentum distribution of fission fragments, *Nucl. Phys. A* **136**, 465 (1969).
- [22] M. M. Hoffman, Directional correlation of fission fragments and prompt gamma rays associated with thermal neutron fission, *Phys. Rev.* **133**, B714 (1964).
- [23] J. B. Wilhelmy, E. Cheifetz, R. C. Jared, S. G. Thompson, H. R. Bowman, and J. O. Rasmussen, Angular momentum of primary products formed in the spontaneous fission of  $^{252}\text{Cf}$ , *Phys. Rev. C* **5**, 2041 (1972).
- [24] Ş. Mişicu, A. Săndulescu, G. M. Ter-Akopian, and W. Greiner, Angular momenta of even-even fragments in the neutronless fission of  $^{252}\text{Cf}$ , *Phys. Rev. C* **60**, 034613 (1999).
- [25] G. F. Bertsch, Reorientation in newly formed fission fragments, *arXiv:1901.00928*.
- [26] G. Scamps, Microscopic description of the torque acting on fission fragments, *Phys. Rev. C* **106**, 054614 (2022).
- [27] G. Scamps and G. Bertsch, Generation, dynamics, and correlations of the fission fragments' angular momenta, *Phys. Rev. C* **108**, 034616 (2023).
- [28] A. Bohr and B. R. Mottelson, Collective and individual-particle aspects of nuclear structure, *Mat. Fys. Medd. Dan. Vid. Selsk.* **27**, 1 (1953).
- [29] R. W. Hasse and W. D. Myers, *Geometric Relationships of Macroscopic Nuclear Physics* (Springer, Berlin, 2011).
- [30] P. Möller, A. J. Sierk, T. Ichikawa, and H. Sagawa, Nuclear ground-state masses and deformations: FRDM (2012), *At. Data Nucl. Data Tables* **109–110**, 1 (2016).

- [31] V. Yu. Denisov and N. A. Pilipenko, Interaction of two deformed, arbitrarily oriented nuclei, *Phys. Rev. C* **76**, 014602 (2007).
- [32] J. Randrup and R. Vogt, Refined treatment of angular momentum in the event-by-event fission model FREYA, *Phys. Rev. C* **89**, 044601 (2014).
- [33] F.-J. Hambsch and S. Oberstedt, Investigation of the far asymmetric region in  $^{252}\text{Cf}(\text{sf})$ , *Nucl. Phys. A* **617**, 347 (1997).
- [34] R. P. Feynman, *Feynman Lectures on Physics* (Addison Wesley, Reading, MA, 1963), Vol. I, Sec. 9.6.